Core-shell gelatin-chitosan nanoparticles with lysozyme responsiveness formed via pH-drive and transglutaminase cross-linking

Jilong Li, Yongqiang Zhao, Yi Zhang, Corinne Nardin

International Journal of Biological Macromolecules 292 (2025) 138802

Contents lists available at ScienceDirect

International Journal of Biological Macromolecules

journal homepage: www.elsevier.com/locate/ijbiomac

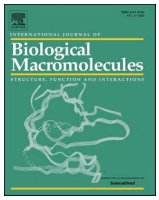

Core-shell gelatin-chitosan nanoparticles with lysozyme responsiveness formed via pH-drive and transglutaminase cross-linking

Jilong Li [a], Yongqiang Zhao [b,**], Yi Zhang [c,***], Corinne Nardin [a,*]

[a] Universite de Pau et des Pays de l'Adour, E2S UPPA, CNRS, IPREM, Pau 64000, France
[b] Key Laboratory of Aquatic Product Processing, Ministry of Agriculture and Rural Affairs, National R&D Center for Aquatic Product Processing, South China Sea Fisheries Research Institute, Chinese Academy of Fishery Sciences, Guangzhou 510300, China
[c] Department of Food Science, The Pennsylvania State University, University Park, PA 16802, USA

ARTICLE INFO

Keywords:
Curcumin
Chitosan
Gelatin
Nanoparticle
Lysozyme

ABSTRACT

Lysozyme-responsive nanoparticles were fabricated using a hydrophilic protein (gelatin type A) as the core and a hydrophobic polysaccharide (chitosan) as the shell. In this study, curcumin was used as a model molecule for encapsulation and promoted the aggregation of gelatin nanoparticles. Transglutaminase catalyzed both intra-molecular cross-linking within gelatin and inter-molecular cross-linking between gelatin and chitosan. The formation mechanism of gelatin nanoparticles was investigated by molecular docking simulations, circular dichroism spectroscopy, UV–vis spectroscopy, turbidity analysis, and dynamic light scattering. Results indicated that pH-driven processes can induce molecular conformational changes of gelatin. However, these alone are insufficient to induce nanoparticle formation. Hydrogen bonding, Pi-alkyl interactions, Pi-Pi interactions, and van der Waals forces between gelatin and curcumin are crucial for the core formation. The coating mechanism of chitosan involved covalent bonds catalyzed by transglutaminase and electrostatic interactions, verified by dynamic light scattering and Fourier transform infrared spectroscopy. Physicochemical properties characterization revealed that the core-shell nanoparticles exhibited a maximum encapsulation efficiency of 97.2 ± 0.3 % and an average particle size of 120 ± 21 nm. The core-shell nanoparticles exhibited high thermal and pH stability, with curcumin retention rates exceeding 80 % under acidic, neutral, and weakly alkaline conditions, and detained thermal degradation up to 90 °C. Additionally, lysozyme responsiveness was evaluated by controlled curcumin release with varying lysozyme concentrations, through which enzymatic hydrolysis of chitosan by lysozyme triggered an increased release rate. In summary, core-shell nanoparticles synthesized from gelatin and chitosan may be effective target delivery systems for curcumin.

1. Introduction

Lysozyme (EC 3.2.1.17) is a hydrolytic enzyme in various biological tissues, cells, and body fluids of the human body, such as the intestinal lumen, tears, saliva, wound fluids, and mucus [1,2]. This enzyme can destroy Gram-positive bacteria by breaking the 1,4-β-glycosidic bonds in peptidoglycan, which is the major structural component of the bacterial cell wall [3]. Based on this mechanism, polysaccharides connected by 1,4-β-glycosidic bonds (e.g., bacterial cellulose, peptidoglycan, and chitosan) are used to develop lysozyme-responsive materials [1,4]. These materials are primarily employed in targeted drug delivery systems in lysozyme-rich environments, such as the intestines, oculars, and wounds [1,5]. Current lysozyme-responsive materials have been developed in the forms of films, hydrogels, and microgels, and they face numerous limitations [5,6], which include fabrication complexity, insufficient mechanical strength, and low encapsulation efficiency. In response to these challenges, this study proposes a novel lysozyme-responsive nanoparticle developed with a core-shell structure. Nanoparticles with core-shell structures have unique features, including a straightforward fabrication process, enhanced mechanical properties, and high drug-loading capacity [7–9]. The designed core is intended to offer a biocompatible and biodegradable environment for drug

* Correspondence to: Corinne Nardin, Universite de Pau et des Pays de l'Adour, E2S UPPA, CNRS, IPREM, Pau 64000, France.
** Correspondence to: Yongqiang Zhao, Key Laboratory of Aquatic Product Processing, Ministry of Agriculture and Rural Affairs, National R&D Center for Aquatic Product Processing, South China Sea Fisheries Research Institute, Chinese Academy of Fishery Sciences, Guangzhou 510300, China.
*** Correspondence to: Yi Zhang, Department of Food Science, The Pennsylvania State University, University Park, PA 16802, USA.
E-mail addresses: zhaoyq@scsfri.ac.cn (Y. Zhao), yjz5549@psu.edu (Y. Zhang), corinne.nardin@univ-pau.fr (C. Nardin).

https://doi.org/10.1016/j.ijbiomac.2024.138802
Received 20 June 2024; Received in revised form 16 November 2024; Accepted 14 December 2024
Available online 15 December 2024

encapsulation, whereas the lysozyme-degradable polymer shell is expected to maintain structural integrity and ensure lysozyme responsiveness. The core-shell structure processed with these two polymers aims to harness the individual advantages of both, offering a promising strategy for creating a more effective and reliable lysozyme-responsive system.

Chitosan is a linear polysaccharide predominantly composed of glucosamine monomers linked by 1,4-β-glycosidic bonds [10]. It is one substrate of lysozyme and thus can be a shell layer that could be degraded by lysozyme in the environment through the catalysis of 1,4-β-glycosidic bonds [1]. In addition, due to its low water solubility, the chitosan shell protects the highly water-soluble core from swelling and disintegrating [11]. Gelatin is a water-soluble protein of low cost, biodegradable, and biocompatible [12], and thus an excellent candidate as the core of the structure. Cross-linking between chitosan and gelatin is essential to enable an efficient lysozyme-responsiveness associated with the shell, and drug release associated with the core. A few cross-linking agents, such as glutaraldehyde, genipin, and transglutaminase (TGase, EC 2.3.2.13) could theoretically cross-link chitosan and gelatin, by utilizing the amine groups in chitosan and the amino acid side chains in gelatin [13,14]. Among the cross-linking agents, TGase-catalyzed cross-linking is safe, and suitable for food, pharmaceuticals, and biomedical applications [15,16]. In the case of cross-linking chitosan and gelatin, TGase can catalyze the covalent bond formation between the carboxyl group of proteins and the amino group of chitosan [17]. To date, TGase has been reported to prepare gelatin-chitosan-based films, hydrogels, gels, and copolymers [17,18]. However, the preparation of gelatin-chitosan-based nanoparticles using TGase has not been reported.

For a core-shell material, the core component contains drugs or other bioactive compounds to enable the function of the material. Curcumin, a hydrophobic polyphenol extracted from *Curcuma longa* [19], offers biological benefits such as anti-inflammatory, antioxidant, antimicrobial, immunomodulatory, and anticancer effects [20,21], but possesses poor water solubility, chemical instability, and limited oral bioavailability [22]. Encapsulating curcumin within nanoparticles produced using proteins, including casein, whey protein, ovalbumin, soy protein isolate, and zein, presents potential to overcome these challenges [23–27]. There have been several conventional methods (e.g., emulsification-solvent evaporation, desolvation, and nanoprecipitation) for preparing gelatin nanoparticles; however, they require the use of significant quantities of organic solvents like acetone and ethanol that are potential hazards [13,28]. A pH-driven method (or pH-cycle, pH-shifting) has been developed for protein nanoparticle preparation, typically hydrophobic proteins [29]. In brief, the neutral pH is at first adjusted to an alkali pH to solubilize and unfold the protein, and subsequently, the pH is readjusted to its initial value, where hydrophobic proteins would form sufficiently strong hydrophobic interactions that drive self-assembly [30]. A recent study has successfully embedded curcumin in gelatin nanoparticles for the first time using the pH-driven method to prepare Pickering emulsions [31], in which curcumin molecules adhere to protein surfaces through a simple complexation process and are embedded within the interior of protein-assembled nanoparticles [32].

In this study, novel lysozyme-responsive nanoparticles with chitosan as shell and gelatin incorporated with curcumin as core were to be formed via a pH-driven and then TGase cross-linking approach. The formation mechanisms of nanoparticles, including the formation of gelatin nanoparticles via the pH-driven process, and the coating of chitosan, were investigated. The properties of the novel nanoparticles were systematically investigated. This study provides theoretical knowledge of eco-friendly synthesis of enzyme responsive nanoparticles designed for curcumin delivery.

2. Materials and methods

2.1. Materials

Gelatin (Type A, from porcine skin), chitosan (medium molecular weight, 86 % degree of deacetylation, purity 75 %, catalogue code 448877), and curcumin (~70 %, HPLC grade) were purchased from Sigma-Aldrich (St. Louis, MO, USA). TGase with an activity of 100 U/g was donated free of charge by Ajinomoto (Tokyo, Japan). Other chemicals were of analytical grade.

2.2. Preparation of CGNPs

2.2.1. Preparation of curcumin-loaded gelatin nanoparticles

Curcumin-loaded gelatin nanoparticles (GNPs) were prepared according to the pH-driven method with little modification [30]. Briefly, gelatin type A (0.3 g) was dissolved in 50 mL of deionized water to form a gelatin solution. The pH of the solution was then raised to 12 with the addition of 1 mol/L NaOH. After stirring at 400 rpm for 5 min, 7.5, 15, 22.5, 30, and 37.5 mg of curcumin were added to form GNPs at various mass ratios (1:40, 2:40, 3:40, 4:40, and 5:40; curcumin to gelatin mass ratio), and the pH was subsequently adjusted to 7.0 using 1 mol/L HCl. The resulting mixture was continuously stirred for 4 h to generate a curcumin-loaded gelatin nanoparticles suspension, and those samples were used for analyzing the GNP formation mechanism (Sections 2.3.1.4 and 2.3.1.5). Based on the results, GNPs were prepared using gelatin solutions at pH 12, with 37.5 mg of curcumin introduced at a mass ratio of 5:40, then neutralized to pH 7.0 for core-shell nanoparticle preparation.

2.2.2. Preparation of chitosan-coated nanoparticles

To prepare chitosan-coated gelatin nanoparticles (CGNPs), 0, 1.5, 3.0, 4.5, and 6.0 mL of chitosan solution (0.3 % *w/v* of chitosan, 1 % *v/v* of acetic acid) was added to 50 mL of the suspension described in Section 2.2.1. and stirred for 2 h at 400 rpm. Subsequently, the pH of the mixture was adjusted to 7 by adding 1 mol/L NaOH. An amount of 225 mg of TGase was added to the mixture, the obtained solution was stirred at 40 °C, 400 rpm for 4 h. Then, the solution pH was adjusted to 1.5 for 30 min to inactivate TGase. Finally, the acidified solution pH was adjusted to 7 before freeze-drying (CRIOS-80, Cryotec, France). These samples were used for formation and property characterizations. Based on the results, 6.0 mL of a chitosan solution with a concentration of 0.3 % *w/v* added to 50 mL of the suspension described in Section 2.2.1 was used for core-shell nanoparticle preparation.

2.3. Mechanism of structure formation

2.3.1. Formation of GNPs

2.3.1.1. Molecular docking. Molecular docking was performed using AutoDockTools-1.5.7 [33]. The crystal structure of collagen type I alpha 1 chain [*Sus scrofa*] (Q6H2X9) was retrieved from the database (https://alphafold.ebi.ac.uk/). Collagen structures at pH 12, 11, 10, 9, 8, and 7 were simulated using H++ (http://newbiophysics.cs.vt.edu/H++/index.php). The 3D structure of curcumin (PubChem CID 969516) was acquired from PubChem (https://pubchem.ncbi.nlm.nih.gov/) and optimized using MM2 force field structure to achieve an energy-minimized conformation. Initially, PyMol 1.8 was employed to remove any solvent and organic molecules from collagen type I [34]. Subsequently, AutoDockTools was used to convert the ligand and receptor files into pdbqt format. In the docking study, Autodock Vina-1.2.5 was used for the simulations of collagen type I-curcumin. Finally, visual docking results were analyzed using Discovery Studio 2019.

2.3.1.2. Circular dichroism spectroscopy (CD). CD spectra of gelatin

solutions and gelatin/curcumin solutions were recorded with a JASCO J-1500 spectrophotometer (Jasco Corporation, Japan). Gelatin and gelatin/curcumin solutions were prepared with pH values adjusted from 12 to 7, containing a protein concentration of 0.3 mg/mL and a curcumin concentration of 0.0375 mg/mL. The sample spectral band in the 190–260 nm range was recorded with a path length of 0.1 cm and a step size of 0.2 nm.

2.3.1.3. UV–vis spectroscopy. UV–vis spectroscopy (UV-2450, Shimadzu, Japan) in the 220–700 nm wavelength range was monitored for three sample types: gelatin solutions with pH adjusted from 12 to 7, gelatin/curcumin solutions with pH adjusted from 12 to 7, and native gelatin solutions.

2.3.1.4. Turbidity. The turbidity of gelatin nanoparticle suspensions was measured following a reported procedure [25]. The absorbance of gelatin solution and GNPs at various gelatin to curcumin mass ratios was measured at 500 nm using a UV–vis spectrophotometer with a 1 cm path length cuvette.

2.3.1.5. Particle size and zeta potential. The particle size, polydispersity index (PDI), and zeta potential of GNPs at various gelatin to curcumin mass ratios were measured by a Zetasizer Nano-ZS (Malvern, UK) at 25 °C (wavelength, λ = 632 nm). The measurement was performed five times and its duration was 60 s.

2.3.2. Formation of CGNPs

2.3.2.1. Particle size and zeta potential. The particle size, PDI, and zeta potential of CGNPs at various chitosan to gelatin mass ratios were measured as described in Section 2.3.1.5.

2.3.2.2. Attenuated total reflectance (ATR) - Fourier transform infrared (FT-IR) spectroscopy. The curcumin, gelatin, chitosan, GNPs, CGNPs without cross-linking, and CGNPs cross-linked by TGase were characterized with a Nicolet ® iS 50 FT-IR spectrometer (Thermo Fisher Scientific, United States) in the ATR mode. The frequency range was 400–4000 cm^{-1}.

2.4. Property characterization of CGNPs

2.4.1. Morphological studies

The morphology of CGNPs was observed with an Apreo 2 S LoVac field emission scanning electron microscope (FESEM) equipped with a comprehensive set of electron detectors for scanning (SEM) and scanning-transmission electron microscopy (STEM) (Thermo Fisher Scientific, United States). Before analysis, a drop of each sample was deposited onto a carbon-coated copper grid and dried.

2.4.2. Encapsulation efficiency (EE) and loading capacity (LC)

The EE and LC of curcumin in the nanoparticles were measured following Niu's method [25]. Briefly, 0.5 mL of the curcumin-loaded nanoparticle suspension was centrifuged at 10,000 rpm for 15 min. After discarding the supernatant, 9 mL of anhydrous ethanol was added. Subsequently, the resulting mixture was ultrasonicated for 2 h and centrifuged at 10,000 rpm for 15 min. The curcumin content in the supernatant was determined at 426 nm using UV–vis spectrophotometry and calculated according to the following standard curve:

$$y = 158.9x + 0.018, R^2 = 0,9999 \quad (1)$$

where y is absorbance, x is the concentration of curcumin (mg/mL), and R^2 is the correlation coefficient.

The EE and LC were calculated using the following equations:

$$EE(\%) = \frac{M_1}{M_2} \quad (2)$$

$$LC(\%) = \frac{M_1}{M_3} \quad (3)$$

where M_1 is the mass of encapsulated curcumin, M_2 is the total mass of added curcumin, and M_3 is the mass of freeze-dried nanoparticles.

2.4.3. Thermal analysis

Thermal analysis of curcumin, gelatin, chitosan, and CGNPs was investigated using thermogravimetric analysis (TGA) and differential scanning calorimetry (DSC). Pyrolysis response of the samples was evaluated by a TGA 2 equipped with a STARe system (Mettler-Toledo, Switzerland) under a N_2 flow from 30 to 600 °C at a rate of 10 °C/min. DSC analysis was conducted using a DSC 3 equipped with the STARe system (Mettler-Toledo, Switzerland), under a constant nitrogen purge of 20 mL/min (25–200 °C).

2.4.4. Stability assessment

The stability of CGNPs was assessed through visual inspection, thermal stability, and pH stability measurements [35].

For storage stability evaluation, CGNPs were stored at 25 °C for 10 and 30 days in the dark. The storage stability was determined by observing precipitation in the samples.

To investigate thermal stability, CGNPs and curcumin were heated for 30 min in a constant-temperature water bath at 70, 80, and 90 °C. The pH stability was studied by storing CGNPs and curcumin at a constant temperature of 20 °C at various pH values (3, 5, 7, 9, and 11) over 30 days. The amount of residual curcumin was determined using the UV–vis spectrophotometer and calculated according to Eq. (1). The thermal and pH stability of CGNPs was expressed by the retention rate (RR) of curcumin:

$$RR(\%) = \frac{M_4}{M_1} \quad (4)$$

where M_1 is the mass of encapsulated curcumin, M_4 is the mass of residual curcumin.

2.4.5. Evaluation of lysozyme responsiveness

The release profile of CGNPs was utilized to investigate their lysozyme responsiveness. Phosphate buffer solution (PBS) at pH 7 and lysozyme concentrations of 0, 0.1, and 1 mg/mL were pre-incubated at 37,0 ± 0.5 °C for 15 min. Then, CGNPs were introduced into these solutions under orbital shaking. Subsequently, samples were taken at 1 h intervals for analysis to assess the release rate, expressed as the percentage of curcumin released from the gelatin core.

2.5. Statistical analysis

The data are presented as (mean ± standard deviation). Statistical analysis was conducted using the Student's *t*-test (comparisons between two groups) and one-way analysis of variance (ANOVA, comparisons among more than two groups) in SPSS 26, with significance at $p < 0.05$.

3. Results and discussion

3.1. Formation of GNPs

3.1.1. Interaction simulation

Molecular docking was performed to investigate interactions between curcumin and collagen type I alpha 1 chain which is the primary composition of gelatin [36,37]. Curcumin exhibits three acidity constants for its ionization steps, i.e., pK_{a1} (7.80), pK_{a2} (8.55), and pK_{a3} (9.05). In the pH range of 12 to 10, curcumin predominantly exists as

A^{3-}, while at pH values of 9, 8, and 7, it mainly exists as HA^{2-}, H_2A^-, and H_3A, respectively [38] (Fig. S1). These respective curcumin forms were employed for molecular docking simulations at specific pH values. Furthermore, because there is one binding site on gelatin for curcumin [31], we conducted the molecular docking simulation using a 1:1 M ratio of curcumin to gelatin. Fig. 1 shows the presence of van der Waals forces, conventional hydrogen bonds, and Pi-Alkyl interactions between curcumin and gelatin across the whole pH range. From pH 12 to 7, their binding energies were similar, −6.5, −6.5, −6.8, −6.7, −6.4, and−6.5 kcal/mol, respectively. At pH 12, curcumin engages in Pi-Sigma interactions with specific amino acid residues. At pH 11, it forms carbon hydrogen bonds, Pi-Pi stacks, and Pi-Pi T-shaped interactions. At pH 10 and 9, curcumin participates in a carbon hydrogen bond, Pi-Sigma, and Pi-Pi stacking interactions. At pH 8 and 7, curcumin exhibits Pi-Pi stacking interactions and Pi-Pi T-shaped interactions. These results suggest that in the pH-driven process, curcumin bound to gelatin via hydrogen bonds, Pi-Alkyl interactions, Pi-Pi interactions, and van der Waals forces, similar to previous reports on other types of gelatin and curcumin [31]. In addition, the dominant interaction forces between curcumin and gelatin were different at different pH values used in the process.

3.1.2. Secondary structure

CD spectroscopy was used to qualitatively analyze the conformational transitions of gelatin in the complexation with curcumin across various pH values. Fig. 2A and B show the CD spectra for gelatin in the presence and absence of curcumin, respectively. All CD spectra exhibit two peaks: a negative peak approximately at 200 nm, indicating a random coil conformation, and a positive peak at approximately 222 nm, corresponding to the triple helix conformation of gelatin [39]. In Fig. 2A, the negative peak exhibits a blue shift from 205 nm to 198 nm as the sample pH decreased from 12 to 10. This indicates a conformational transition of gelatin towards more ordered structures, which might be because pH 12 is much higher than the pI of gelatin, their molecules are negatively charged, leading to intermolecular repulsion. Lowering the pH reduced this charge, decreased repulsion, and potentially increased intermolecular interactions such as hydrogen bonding and hydrophobic interactions. Consequently, this may result in a more compact arrangement of random coil structures or the emergence of more ordered structural regions within the gelatin molecules. Besides, pH adjustments could facilitate the formation or increase the prevalence of β-sheet structures [40], contributing to the observed changes in the CD spectra. However, for gelatin/curcumin solutions (Fig. 2B), a blue shift was observed only when the pH was adjusted from 12 to 11. This suggested that curcumin might promote the ordering of the gelatin structure between pH 12 and 11. At these pH, weak positive peaks at 222 nm were observed in the CD spectra of the gelatin/curcumin solution compared to the gelatin solution which exhibits no positive peak. This can be attributed to the promoting effect of curcumin on the restoration of gelatin's triple helix structure. The principal internal hydrogen bonding within the triple helix contributes to the stability of the structure [41]. Molecular docking simulations in Section 3.1.1. predicted that curcumin acted as a hydrogen bond acceptor within gelatin molecules under highly alkaline conditions, reassembling part of its triple helix structure. Notably, no significant change was observed in the random coil conformation peak between the gelatin solution and the gelatin/curcumin solution at other pH values, which strongly suggests structure stabilization of gelatin molecules. Moreover, all negative peaks were observed at 198 nm, indicating that curcumin does not alter the secondary structure of gelatin between pH 7 and 10.

3.1.3. Conformational features

UV–vis spectroscopy was employed to analyze gelatin interactions with curcumin in the microenvironment. As shown in Fig. 2C, the absorption peaks of gelatin in the range of 270–310 nm are attributed to the absorption of carbon backbones and amino acid residues [23]. When the pH of native gelatin was adjusted to 12, there was an enhancement in the absorbance of these peaks, which was linked to the exposure of

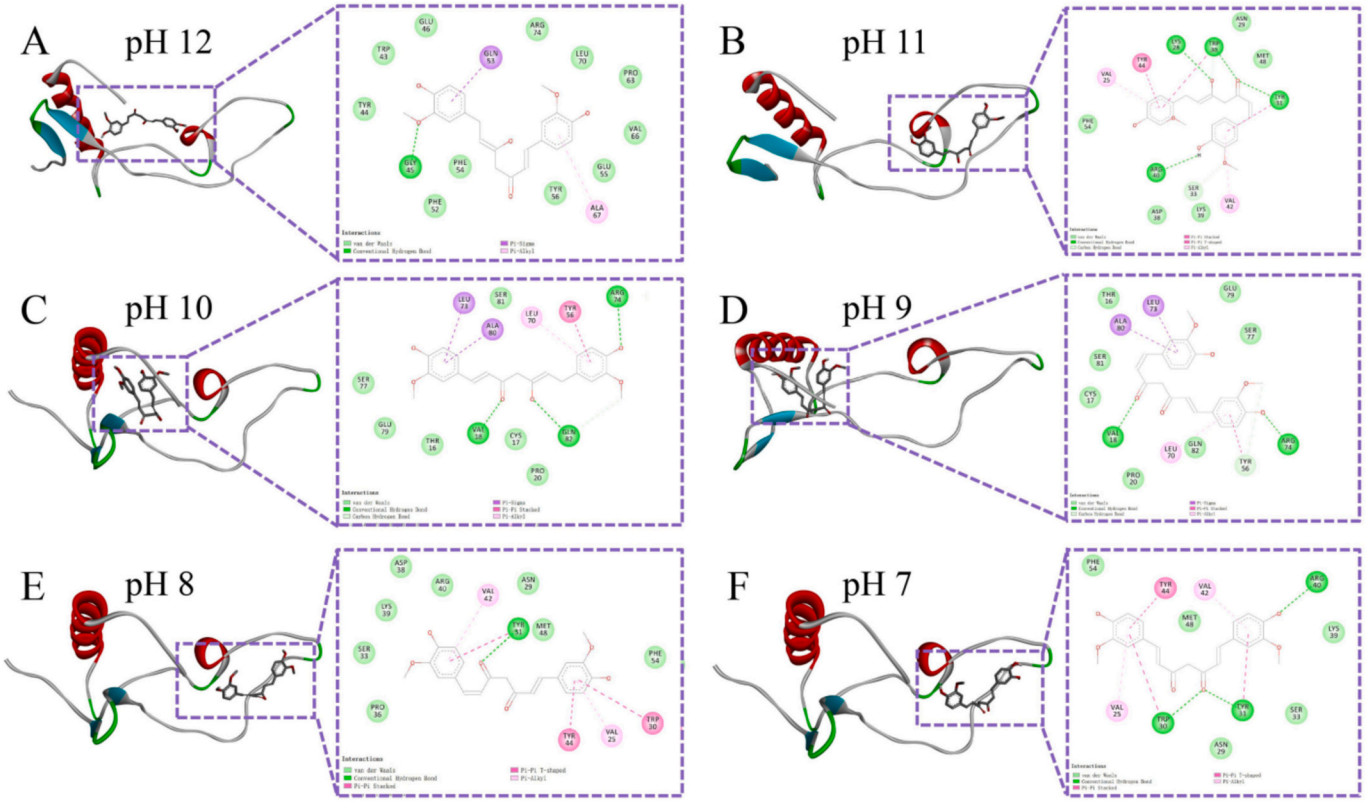

Fig. 1. Molecular docking results of curcumin on collagen type I alpha 1 chain at pH 12 (A), 11 (B), 10 (C), 9 (D), 8 (E), and 7 (F).

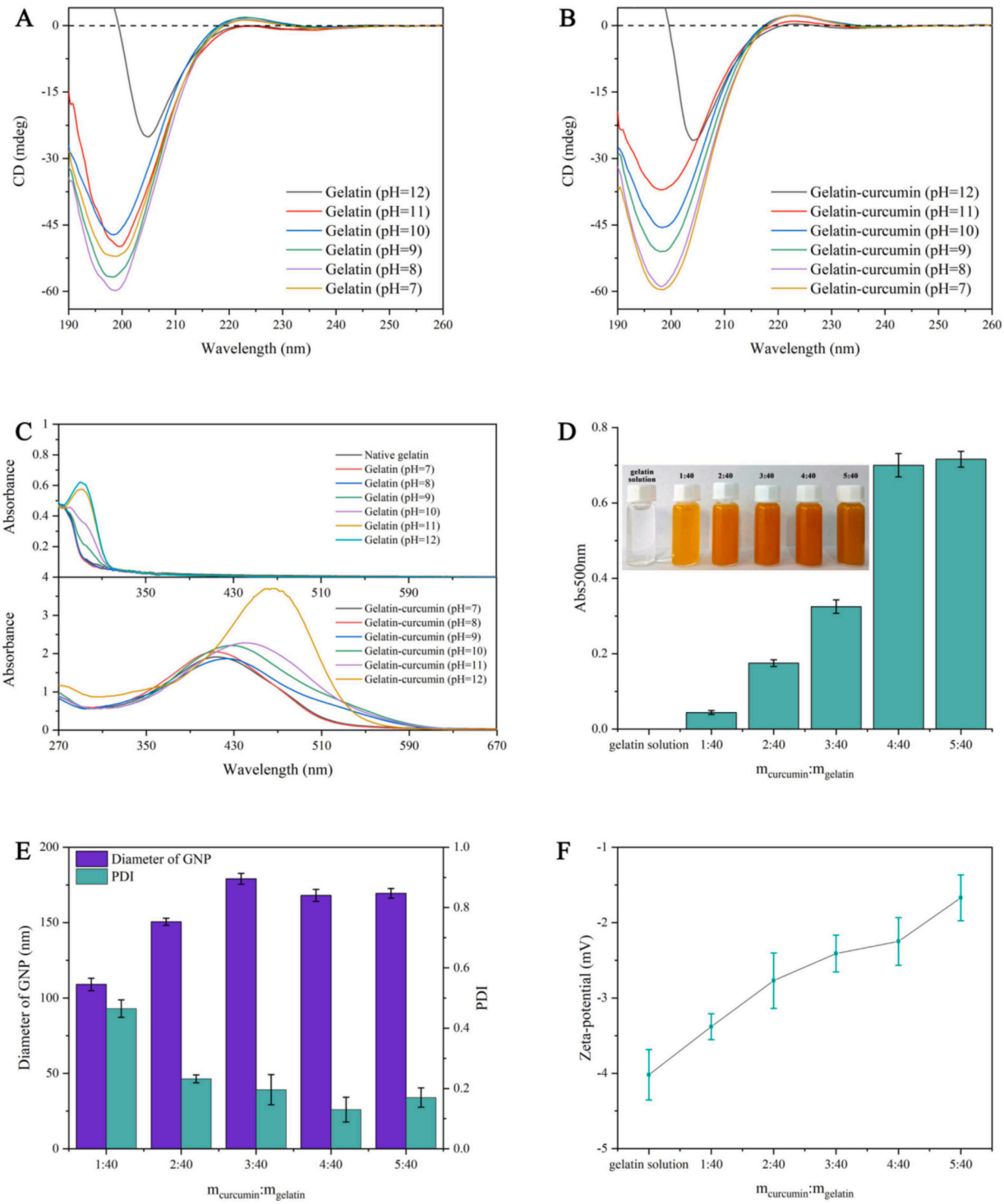

Fig. 2. Experimental characterization of the formation mechanism of GNPs: CD spectra of gelatin solution (A) and gelatin/curcumin solution (B) at different pH; UV–vis absorption spectra of gelatin solution and gelatin/curcumin solution at different pH (C); effect of curcumin/gelatin mass ratio on the turbidity (D), diameter (E), and zeta-potential (F) of GNPs.

hydrophobic groups and structural modifications [42]. Conversely, when the gelatin was acidified to a lower pH, the intensity decreased, and the spectral features began to resemble those of native gelatin, indicating a partial refolding of the gelatin structure. This trend was not observed in the UV–vis spectra of gelatin/curcumin solutions. The presence of curcumin introduced a new characteristic peak in the 310–590 nm range. This can be attributed to the presence of phenolic compounds and unsaturated bonds, along with electron excitation resulting from the Pi - Pi* transition occurring in curcumin [43]. Moreover, a blue shift (466 nm to 416 nm) was observed as the pH of the gelatin/curcumin solution was adjusted from 12 to 7, which was probably due to the protonation of curcumin in which the enol form predominates in alkaline conditions, whereas the keto form prevails in acidic and neutral environments [44].

3.1.4. Turbidity

Typically, the turbidity of nanoparticle suspensions is contingent on factors such as particle concentration, size, refractive index, and aggregation state [45]. The turbidity of GNP suspensions was investigated at various mass ratios of curcumin to gelatin. As shown in Fig. 2D, samples with ratios of 4:40 and 5:40 exhibited notably high and similar turbidity. However, turbidity showed a sharp decrease when the ratio of curcumin decreased further. The turbidity of the solution in the absence of curcumin was 0. This finding differed from the pH-driven method on soy protein isolate, which formed nanoparticles without interactions with small molecular drugs [23]. It suggests that curcumin probably played a crucial role in GNP formation. It could be assumed that curcumin binds to the hydrophobic pockets within gelatin molecules through a combination of hydrophobic interactions and hydrogen bonds [46], and the interaction enhances the intermolecular attraction between gelatin molecules, thereby promoting molecular aggregation and the production of gelatin nanoparticles.

3.1.5. Particle size and zeta potential analysis

Various mass ratios of curcumin and gelatin were employed to investigate how curcumin influences the characteristics of GNPs. DLS analysis (Fig. 2E) revealed that as the curcumin ratio increased, the GNP size tended to increase from (109 ± 4) nm to (172 ± 6) nm. Furthermore, the PDI of GNPs decreased from (0.47 ± 0.03) to below 0.3. In Fig. S2, an evident multi-peak distribution was observed for GNP-1:40, whereas all other samples exhibit a single-peak distribution. These results suggest that curcumin improves the aggregation of gelatin molecules, leading to the formation of GNPs. Notably, the zeta potential of gelatin type A and overall GNPs was negatively charged below pH 7 (Fig. 2F). Moreover, as the curcumin ratio increased, the zeta potential rose from (−3.4 ± 0.2) mV to (−1.7 ± 0.3) mV. This may be attributed to greater exposure of ions or of chemical functional groups on the surface of GNPs with a low curcumin ratio because of insufficient aggregation of the gelatin molecule, resulting in a lower zeta potential. Conversely, as gelatin molecules aggregate due to interacion with curcumin, these ions and functional groups exposure decreased, which led to an increase in zeta potential.

3.2. Formation of CGNPs

3.2.1. Particle size and zeta potential

The formation of CGNPs by the coating process of GNPs using chitosan was investigated at varying mass ratios of chitosan and gelatin. As shown in Fig. 3A, the diameter of CGNPs gradually increased to (340 ± 14) nm as chitosan was added. In addition, the zeta potential of CGNPs increased upon the introduction of chitosan because of chitosan's positive charge (Fig. 3B). Notably, the zeta potential of CGNPs was close to 0 mV when the chitosan to gelatin mass ratio reached 6:200. At this point, the positive charge of chitosan entirely neutralized the negative charges on the surface of GNPs. As the ratio of chitosan was further increased, the zeta potential of CGNPs eventually reached (+1.2 ± 0.3) mV. This demonstrated that electrostatic interactions play an essential role in the coating process.

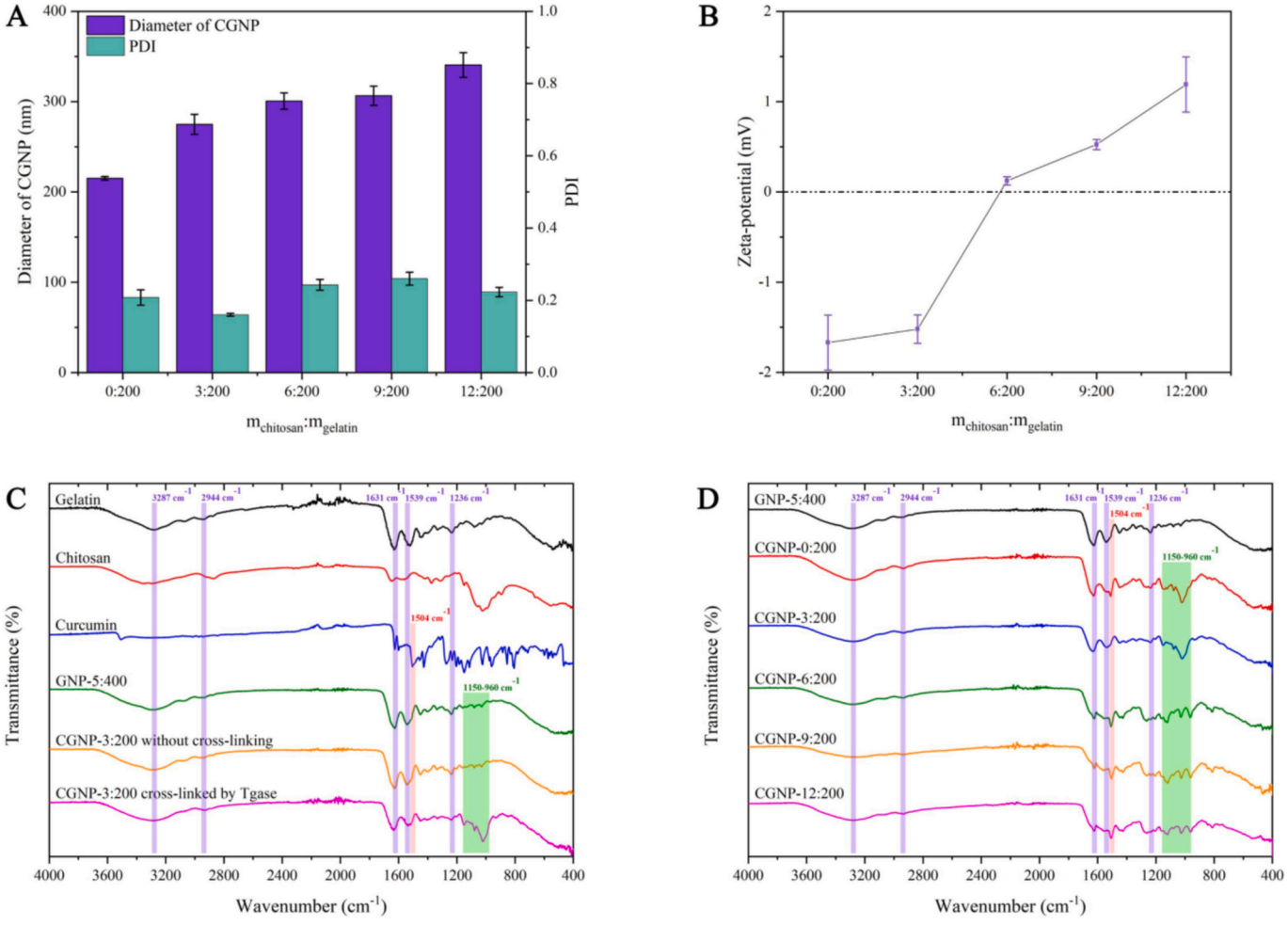

Fig. 3. Formation of CGNPs: effect of chitosan/gelatin mass ratio on the diameter (A) and zeta-potential (B) of CGNPs; the ATR-FT-IR spectra of gelatin, chitosan, curcumin, GNP-5:400, CGNP-3:200 without cross-linking, CGNP-3:200 cross-linked by Tgase (C), and CGNPs at various mass ratios (D).

3.2.2. ATR-FT-IR spectra

The curcumin-loaded nanoparticles with gelatin core and chitosan shell were cross-linked by TGase as confirmed by FT-IR. Fig. 3C shows the FT-IR spectra of gelatin, chitosan, curcumin, GNP-5:40, CGNP-3:200 without cross-linking, and CGNP-3:200 cross-linked by TGase. It was observed that gelatin and GNP-5:40 have similar FT-IR spectra. The bands assigned to O−H and C−H stretching at 3287 and 2944 cm^{-1} were observed. In addition, the spectra showed three prominent amide peaks: amide-I (C═O stretching, 1631 cm^{-1}), amide-II (N−H bending 1539 cm^{-1}), and amide-III (in the plane of vibrations C−N and N−H groups of bound amide or vibrations of CH_2 groups of side chains, 1236 cm^{-1}) [47]. The spectrum of chitosan showed the characteristic bands at 3360 and 3288 cm^{-1} attributable to O−H and N−H stretching, respectively [48]. The bands at 2922 and 2870 cm^{-1} are attributed to the stretching of asymmetric and symmetric C−H groups, respectively [49]. The absorption band at 1653 cm^{-1} corresponds to C═O stretching, and the band at 1583 cm^{-1} is attributable to the N−H deformation of amino groups [50]. The presence of the glucose units of the polysaccharide structure was confirmed from the bands between 1152 and 896 cm^{-1} [51]. Fig. 3D shows the FT-IR spectra of GNP-5:40 and CGNPs at different chitosan/gelatin mass ratios. Splitting and shifting of amino groups in aliphatic amino acids were observed in the 1150–960 cm^{-1} range. Notably, the spectra of CGNP-0:200 and CGNP-3:200 exhibit similarities. It suggested the formation of covalent bonds between the free amino groups and gamma-carboxamide groups of glutamine. Additionally, more obvious changes were observed in the remaining three groups of CGNPs. It suggested that interactions between the carboxyl groups of gelatin and the amino groups of chitosan may also play a role. These bonds formed by TGase contribute to the cross-linking within the gelatin molecule and the cross-linking of the gelatin with chitosan.

FT-IR analysis (Fig. 3C and D) confirmed successful curcumin encapsulation in the nanoparticles, with shoulder peaks for curcumin at 1504 cm^{-1} [31]. The variation in peak intensity primarily arose from the physical interaction between gelatin and curcumin. Compared to GNP-5:40 and CGNP-0:200, a blue shift of approximately 9 or 3 cm^{-1} was observed for 1631 cm^{-1} (C═C stretching vibration, curcumin) and 1539 cm^{-1} (N−H bending, chitosan) peaks in other CGNPs. This may be attributed to the formation of hydrogen bonds between the ketone groups of curcumin and the chitosan molecule. These hydrogen bonds can increase the binding energy of the C═O bond. Furthermore, the hydrogen bond interaction led to an increase in the bond length of N−H, resulting in a blue shift [52]. This result demonstrated that curcumin is not only localized within the gelatin nucleus but also distributed throughout the chitosan shell.

3.3. Properties of CGNPs

3.3.1. Morphological structures

The morphology of CGNPs at various mass ratios of chitosan and gelatin was analyzed by FESEM in the STEM mode. The core-shell structure of CGNP-12:200 was observed in Fig. 4A and C. Imaging of the other CGNP structures in Fig. S3A, C, E, and G did not reveal the core-shell structure, which might be attributed to the insufficient amount of chitosan to form an observable shell coating on the GNPs. All CGNPs exhibited a spherical structure with a smooth surface (Fig. 4A and Fig. S3A, C, E, G). The diameter distribution was assessed using Nano Measurer 1.2, analyzing data from 100 nanoparticles. Subsequently, the mean diameters were determined through normal curve fitting and were shown in Fig. 4B and Fig. S3B, D, F, H. The mean diameter of CGNPs was (120 ± 21) nm. Notably, the diameters of all the CGNPs observed by FESEM were slightly smaller than those measured by DLS, but this phenomenon was also reported by Li [24]. It can be attributed to two factors. Firstly, CGNPs formed predominantly from water-soluble gelatin may swell in aqueous solutions. Secondly, zeta potential results indicated that CGNPs carry an electrical charge on their surface, inducing repulsion in solution and forming an "electric double layer" structure [53]. This long-range Coulomb interaction resulted in larger particle diameters in DLS measurements compared to STEM measurements [54].

3.3.2. EE and LC

Fig. 4D shows the EE and LC of CGNPs at different chitosan/gelatin mass ratios. It was observed that the nanoparticles without chitosan exhibited an EE of curcumin of (87 ± 3)%. As anticipated, the addition of chitosan increased EE. FT-IR results in Section 3.2.2 demonstrated that this increase was attributed to the encapsulation of free curcumin in chitosan. At the chitosan to gelatin mass ratio of 6:200, the EE significantly increased to (97.2 ± 0.3)%. The EE did not change as the mass ratio of chitosan increased. Similarly, the introduction of chitosan increased the LC of curcumin in CGNPs. However, a further increase in the chitosan ratio resulted in a decrease in LC. This decrease was attributed to LC, representing the mass ratio of encapsulated curcumin to the total weight of chitosan and gelatin. These results suggest that chitosan enhances the embedding ability of nanoparticles.

3.3.3. Thermal properties

TGA results and derivative thermogravimetric analysis (DTG) for gelatin, curcumin, chitosan, and CGNPs are depicted in Fig. S4 and 4E. Relevant data are displayed in Table S1. Weight loss (water evaporation) between 30 and 150 °C was observed in all samples except curcumin [6]. Conversely, curcumin remained stable up to 214 °C because of its hydrophobic nature and low water retention capacity. Gelatin weight lost from 204 to 486 °C was due to the decomposition of the collagen-like triple helix structure [55]. Weight loss in chitosan, observed from 228 to 414 °C, corresponded to the decomposition of the pyranose ring, involving the rupture of glycosidic linkages between glucosamine and *N*-acetylglucosamine, and the subsequent release of volatile products [56]. CGNP-0:200 and gelatin exhibited similar characteristic temperature ranges in the second stage. However, after introducing chitosan, the DTG curves of CGNPs showed a slight shoulder peak before the thermal degradation stage of gelatin. This stage showed approximately 4 % weight loss, likely due to the degradation of chitosan. As reported previously, curcumin can modify the structural integrity of chitosan, affecting its thermal stability and degradation behavior [52]. Consequently, the maximum degradation temperature of chitosan was reduced from 306 °C to approximately 240 °C. Overall, CGNPs exhibited a weight loss of 37.9 % to 42.81 % at 600 °C, significantly lower than the 79.94 % and 65.35 % observed for gelatin and chitosan, respectively. This suggests that the enzymatic cross-linking bonds contribute to forming a more stable structure than gelatin and chitosan, thereby enhancing the stability of the nanoparticles.

The results of the DSC further confirmed these conclusions. The denaturation temperature values (T_d) are shown in Fig. 4F and Table S2 as the first endothermic peak. It was attributed to the evaporation of water from the samples and to the helix-to-coil transition in gelatin [57]. The T_d end values of CGNPs were higher than gelatin T_d. This was related to the enhanced thermal stability of the nanoparticles due to cross-linking [58]. Additionally, the DSC results from the second heating run (Table S2) revealed that the glass transition temperature values (T_g) of CGNPs were higher than the one of gelatin, ranging from 182.67 °C to 184.61 °C. T_g is generally associated with the molecular segmental motion in amorphous structures [58]. The higher T_g can be explained by increased cross-linking due to the inclusion of TGase, which reduced the free volume and restricted the molecular mobility of gelatin [57]. Notably, the DSC curves from the first heating run exhibited the same endothermic crystalline melting point peak as curcumin at 175 °C. It suggested that curcumin remains in its crystalline form within the CGNPs.

3.3.4. Stability

Fig. S5 shows the visual appearance of CGNPs stored in the dark at

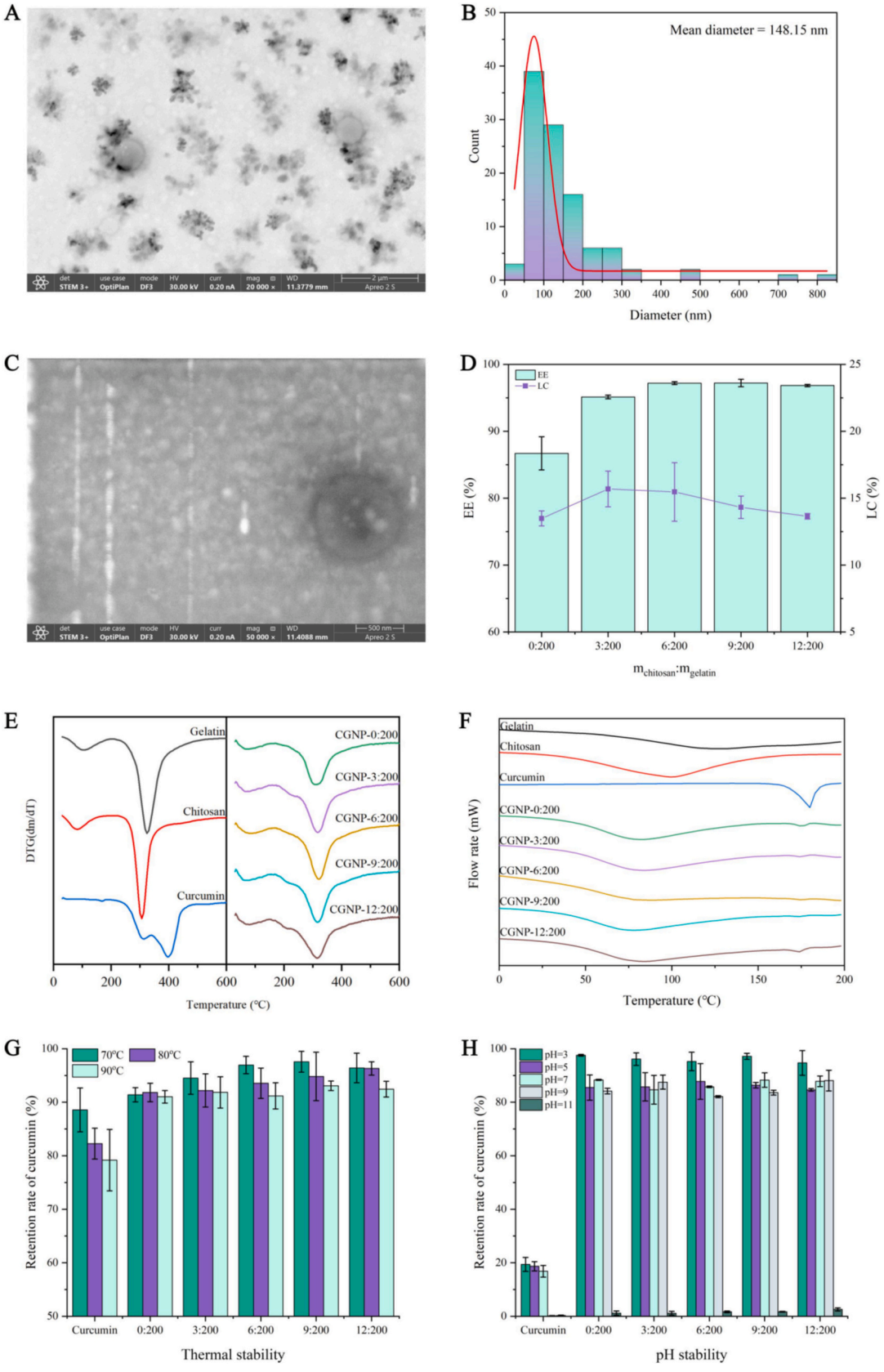

Fig. 4. Properties of CGNPs: the STEM image (A) and mean diameter (B) of CGNP-12:200 with 20,000× magnification, and its STEM image with 50,000× magnification (C); the encapsulation efficiency and loading capacity of CGNPs with different chitosan/gelatin mass ratios (D); the DTG (E) and DSC (F) of gelatin, chitosan, curcumin, and CGNPs; the thermal (G) and pH stability (H).

room temperature for 10, 20, and 30 days. No significant changes were observed in all samples from 0 to 10 days. Small sediments could be observed after 20 and 30 days of storage. Therefore, the nanoparticles exhibited good stability. Generally, nanoparticles exhibiting zeta potentials greater than ±30 mV offer adequate electrostatic repulsion to inhibit particle aggregation and maintain suspension stability [59]. Consequently, the low zeta potential of CGNPs, as presented in Section 3.2.1, indicated reduced electrostatic stabilization. This reduction theoretically enhanced the probability of particle aggregation and precipitation. Under identical storage conditions, a suspension of GNPs without TGase cross-linking exhibited significant aggregation and gelation after 24 h of storage. This is similar to the phenomenon in GNP suspensions prepared using bovine bone gelatin [30]. The good stability of CGNPs could be attributed to the enhanced structural integrity of the enzyme cross-linked nanoparticles as confirmed by TGA and DSC. Compared with uncross-linked GNPs, aggregation and disintegration were less likely during storage.

The thermal and pH stability of CGNPs was quantified by the RR of curcumin. As shown in Fig. 4G, the RR of free curcumin decreased to (89 ± 5)%, (82 ± 3)%, and (79 ± 6)% after heating at 70, 80, and 90 °C for 30 min, respectively. As expected, the RR of curcumin embedded in nanoparticles was higher. Moreover, nanoparticles coated with chitosan exhibited a high RR of curcumin compared to CGNP-0:200, and the RR increased slightly with the increase in chitosan ratio ($p < 0.05$). When the ratio of chitosan to gelatin reached 9:200, the RR reached (98 ± 2)%, (95 ± 5)%, and (93.1 ± 0.9)% after heating at 70, 80, and 90 °C, respectively. As a result, CGNPs could protect curcumin from thermal treatment. In Fig. 4H, the stability variation with pH is presented. After 30 days of storage at pH 3, 5, and 7, the RR of free curcumin decreased to around 20 %. Conversely, the RR of curcumin for CGNPs remained above 80 % in both acidic and neutral conditions. In addition, the RR at pH 3 was significantly higher than those at other pHs ($p < 0.05$). At pH 9, the RR of free curcumin approached 0, while CGNPs still exhibited protection. The RR of curcumin embedded in CGNPs at pH 9 ranged from (82.1 ± 0.4)% to (88 ± 4)%. However, the RR of CGNPs was also close to 0 % at pH 11. This is because gelatin dissolves in solution under these conditions to the extent that it cannot protect the curcumin. The above results indicated that CGNPs had excellent stability under acidic, neutral as well as weakly alkaline conditions. Besides, the pH stability of the different types of CGNPs was similar ($p > 0.05$) under the same pH.

3.3.5. *Lysozyme responsiveness*

The lysozyme responsiveness of CGNPs was investigated by analyzing the curcumin release rates at 6 h (Fig. 5A) and release profile (Fig. 5B, C, and D) at lysozyme concentrations of 0, 0.1, and 1 mg/mL. In a lysozyme-free environment, significant differences ($p < 0.05$) were observed in the release rates of various CGNPs over 6 h. The maximum release rate observed was (66 ± 2)% for CGNP-0:200. With an increasing chitosan ratio, the release rate of curcumin at 6 h gradually decreased to around 40 %. This proved that the chitosan coating effectively slows down the curcumin release rate. As shown in Fig. 5C, this trend persisted at lysozyme concentrations of 0.1 mg/mL. In contrast, the release rate of chitosan-containing nanoparticles increased. Notably, Fig. 5D revealed that the release rates of CGNPs at 6 h did not significantly differ ($p > 0.05$) when the lysozyme concentration was increased to 1 mg/mL. This could be attributed to the catalytic hydrolysis of 1,4-β-glycosidic bonds in chitosan by lysozyme [1], resulting in a loss of its ability to protect the gelatin cores. The above results confirmed that chitosan could influence curcumin release and give CGNPs lysozyme-responsiveness.

4. Conclusion

In this study, CGNPs with a core-shell structure were prepared by a toxic organic solvent-free method, combining pH-drive and TGase cross-linking. The optimal mass ratio for the preparation was 25:12:200 (curcumin:chitosan:gelatin). Their structure formation mechanisms and properties were investigated. The structure of gelatin type A became more ordered as the solution's pH adjusted from strongly alkaline to close to the gelatin's pI. Concurrently, curcumin facilitated the formation of GNPs by influencing the gelatin microenvironment, promoting molecular aggregation, and altering the structural conformation of gelatin. This process primarily involved a variety of non-covalent bonds, including hydrogen bonding, Pi-alkyl interactions, Pi-Pi interactions, and van der Waals forces. Subsequently, the chitosan shell structure of the nanoparticles was developed through covalent bonds catalyzed by TGase and electrostatic interactions. The CGNPs demonstrated improved encapsulation efficiency from 87 % to 97 %, and high thermal and pH stability, retaining over 80 % of curcumin under acidic, neutral, and weakly alkaline conditions, and detained thermal degradation up to 90 °C. Besides, the chitosan shell endowed them with lysozyme responsiveness. The release rate increased from approximately 40 % to over 66 % within 6 h in the presence of lysozyme, suggesting a positive correlation with lysozyme concentration. This responsiveness is attributed to the enzymatic hydrolysis of chitosan, which effectively triggers the release. These results indicated that the designed CGNPs possess potential application prospects in drug delivery for organs in which lysozyme exists, such as the intestines, oculars, and wounds. Future research would focus on exploring the bioaccessibility, biocompatibility, and in vivo and in vitro drug release kinetics of CGNPs to validate their clinical potential for practical applications.

CRediT authorship contribution statement

Jilong Li: Writing – original draft, Methodology, Investigation, Formal analysis, Conceptualization. **Yongqiang Zhao:** Writing – review & editing, Investigation, Funding acquisition, Data curation. **Yi Zhang:** Writing – review & editing, Visualization, Validation, Supervision, Resources, Project administration, Methodology, Funding acquisition, Data curation, Conceptualization. **Corinne Nardin:** Writing – review &

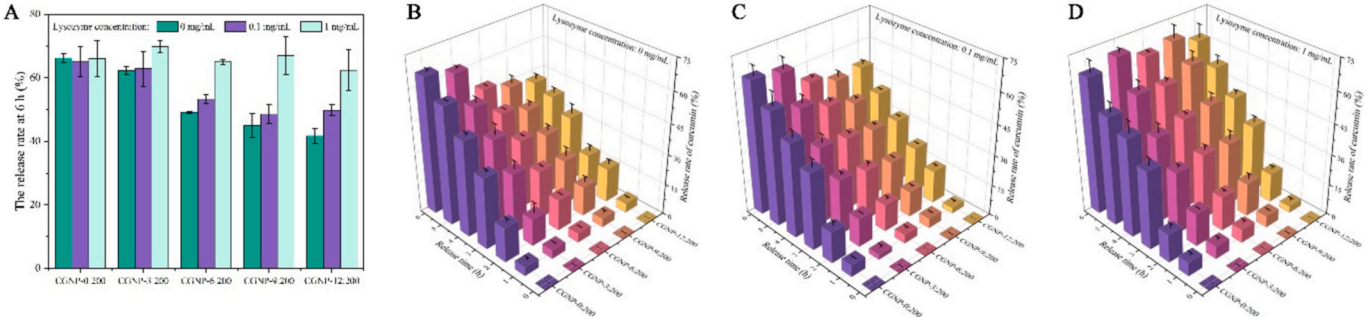

Fig. 5. (A) The curcumin release rates at 6 h of CGNPs with different chitosan/gelatin mass ratios. Curcumin release rate in PBS buffer at lysozyme concentrations of 0 (B), 0.1 (C), and 1 mg/mL (D).

editing, Visualization, Validation, Supervision, Resources, Project administration, Methodology, Funding acquisition, Data curation, Conceptualization.

Declaration of competing interest

The authors declare that they have no known competing financial interests or personal relationships that could have appeared to influence the work reported in this paper.

Acknowledgments

The work was funded by I-SITE E2S with Aid award agreement No. ANR-16-IDEX-0002. This research was also supported by the United States Department of Agriculture (USDA) National Institute of Food and Agriculture and Hatch Appropriations under the Accession number 7005076. Circular dichroism spectroscopy (CD) assays were supported by the Central Public-interest Scientific Institution Basal Research Fund, CAFS (2023TD78). This work was also financially supported by the European Union's Horizon 2020 research and innovation program under the Marie Sklodowska-Curie programme (grant agreement No 823883). J. Li acknowledges a scholarship from the China Scholarship Council (CSC) (202208220048).

Supplementary data

Supplementary data to this article can be found online at https://doi.org/10.1016/j.ijbiomac.2024.138802.

Data availability

Data will be made available on request.

References

[1] X. Li, L. Hetjens, N. Wolter, H. Li, X. Shi, A. Pich, Charge-reversible and biodegradable chitosan-based microgels for lysozyme-triggered release of vancomycin, J. Adv. Res. 43 (2023) 87–96, https://doi.org/10.1016/j.jare.2022.02.014.
[2] N. Nawaz, S. Wen, F. Wang, S. Nawaz, J. Raza, M. Iftikhar, M. Usman, Lysozyme and its application as antibacterial agent in food industry, Molecules 27 (2022) 6305, https://doi.org/10.3390/molecules27196305.
[3] G. Leśnierowski, T. Yang, Lysozyme and its modified forms: a critical appraisal of selected properties and potential, Trends Food Sci. Technol. 107 (2021) 333–342, https://doi.org/10.1016/j.tifs.2020.11.004.
[4] P.M. Alves, C.C. Barrias, P. Gomes, M.C.L. Martins, Smart biomaterial-based systems for intrinsic stimuli-responsive chronic wound management, Mater. Today Chem. 22 (2021) 100623, https://doi.org/10.1016/j.mtchem.2021.100623.
[5] M. Åhlén, G.K. Tummala, A. Mihranyan, Nanoparticle-loaded hydrogels as a pathway for enzyme-triggered drug release in ophthalmic applications, Int. J. Pharm. 536 (2018) 73–81, https://doi.org/10.1016/j.ijpharm.2017.11.053.
[6] C. Wang, M. Sun, Z. Fan, J. Du, Intestine enzyme-responsive polysaccharide-based hydrogel to open epithelial tight junctions for oral delivery of imatinib against colon cancer, Chin. J. Polym. 40 (2022) 1154–1164, https://doi.org/10.1007/s10118-022-2726-0.
[7] S. Chen, Y. Zhang, J. Qing, Y. Han, D.J. McClements, Y. Gao, Core-shell nanoparticles for co-encapsulation of coenzyme Q10 and piperine: surface engineering of hydrogel shell around protein core, Food Hydrocoll. 103 (2020) 105651, https://doi.org/10.1016/j.foodhyd.2020.105651.
[8] X. Dong, L. Liu, Y. Wang, T. Li, Z. Wu, H. Yuan, P. Ma, D. Shi, M. Chen, W. Dong, The compatibilization of poly (propylene carbonate)/poly (lactic acid) blends in presence of core-shell starch nanoparticles, Carbohydr. Polym. 254 (2021) 117321, https://doi.org/10.1016/j.carbpol.2020.117321.
[9] M.M. Leena, T. Anukiruthika, J.A. Moses, C. Anandharamakrishnan, Co-delivery of curcumin and resveratrol through electrosprayed core-shell nanoparticles in 3D printed hydrogel, Food Hydrocoll. 124 (2022) 107200, https://doi.org/10.1016/j.foodhyd.2021.107200.
[10] H. Lin, T. Li, B.J. Janani, A. Fakhri, Fabrication of Cu_2MoS_4 decorated WO_3 nano heterojunction embedded on chitosan: robust photocatalytic efficiency, antibacterial performance, and bacteria detection by peroxidase activity, J. Photochem. Photobiol. B Biol. 226 (2022) 112354, https://doi.org/10.1016/j.jphotobiol.2021.112354.
[11] A. Athipornchai, P. Pabunrueang, T. Trakulsujaritchok, Mangiferin loaded carrageenan/chitosan core-shell hydrogel beads: preparation, characterization and proposed application, Food Hydrocoll. 147 (2024) 109394, https://doi.org/10.1016/j.foodhyd.2023.109394.
[12] Y. Lu, Q. Luo, Y. Chu, N. Tao, S. Deng, L. Wang, L. Li, Application of gelatin in food packaging: a review, Polymers 14 (2022) 436, https://doi.org/10.3390/polym14030436.
[13] A.E. Koletti, E. Tsarouchi, A. Kapourani, K.N. Kontogiannopoulos, A. N. Assimopoulou, P. Barmpalexis, Gelatin nanoparticles for NSAID systemic administration: quality by design and artificial neural networks implementation, Int. J. Pharm. 578 (2020) 119118, https://doi.org/10.1016/j.ijpharm.2020.119118.
[14] K. Song, B. Ren, Y. Zhai, W. Chai, Y. Huang, Effects of transglutaminase cross-linking process on printability of gelatin microgel-gelatin solution composite bioink, Biofabrication 14 (2021) 015014, https://doi.org/10.1088/1758-5090/ac3d75.
[15] T. Wu, C. Liu, X. Hu, Enzymatic synthesis, characterization and properties of the protein-polysaccharide conjugate: a review, Food Chem. 372 (2022) 131332, https://doi.org/10.1016/j.foodchem.2021.131332.
[16] Y. Zhang, B.K. Simpson, Food-related transglutaminase obtained from fish/shellfish, Crit. Rev. Food Sci. Nutr. 60 (2020) 3214–3232, https://doi.org/10.1080/10408398.2019.1681357.
[17] D.A. Kadimaliev, O.V. Parchaykina, I.V. Syusin, I.V. Chairkin, A.N. Malafeev, A. A. Devyatkin, V.V. Revin, Effect of transglutaminase on the properties of films prepared from chitosan and gelatin, Appl. Biochem. Microbiol. 57 (2021) 366–372, https://doi.org/10.1134/S0003683821030042.
[18] R. Rodríguez-Rodríguez, H. Espinosa-Andrews, C. Velasquillo-Martínez, Z. Y. García-Carvajal, Composite hydrogels based on gelatin, chitosan and polyvinyl alcohol to biomedical applications: a review, Int. J. Polym. Mater. Polym. Biomater. (2020), https://doi.org/10.1080/00914037.2019.1581780.
[19] A. Memarzia, M.R. Khazdair, S. Behrouz, Z. Gholamnezhad, M. Jafarnezhad, S. Saadat, M.H. Boskabady, Experimental and clinical reports on anti-inflammatory, antioxidant, and immunomodulatory effects of *Curcuma longa* and curcumin, an updated and comprehensive review, BioFactors 47 (2021) 311–350, https://doi.org/10.1002/biof.1716.
[20] M.J. Banez, M.I. Geluz, A. Chandra, T. Hamdan, O.S. Biswas, N.S. Bryan, E.R. Von Schwarz, A systemic review on the antioxidant and anti-inflammatory effects of resveratrol, curcumin, and dietary nitric oxide supplementation on human cardiovascular health, Nutr. Res. 78 (2020) 11–26, https://doi.org/10.1016/j.nutres.2020.03.002.
[21] J.J. Ferguson, K.A. Abbott, M.L. Garg, Anti-inflammatory effects of oral supplementation with curcumin: a systematic review and meta-analysis of randomized controlled trials, Nutr. Rev. 79 (2021) 1043–1066.
[22] S. Sabet, A. Rashidinejad, L.D. Melton, D.J. McGillivray, Recent advances to improve curcumin oral bioavailability, Trends Food Sci. Technol. 110 (2021) 253–266, https://doi.org/10.1016/j.tifs.2021.02.006.
[23] H. Li, X. Zhang, C. Zhao, H. Zhang, Y. Chi, L. Wang, H. Zhang, S. Bai, X. Zhang, Entrapment of curcumin in soy protein isolate using the pH-driven method: Nanoencapsulation and formation mechanism, LWT 153 (2022) 112480, https://doi.org/10.1016/j.lwt.2021.112480.
[24] Z. Li, Q. Lin, D.J. McClements, Y. Fu, H. Xie, T. Li, G. Chen, Curcumin-loaded core-shell biopolymer nanoparticles produced by the pH-driven method: physicochemical and release properties, Food Chem. 355 (2021) 129686, https://doi.org/10.1016/j.foodchem.2021.129686.
[25] F. Niu, D. Hu, F. Gu, Y. Du, B. Zhang, S. Ma, W. Pan, Preparation of ultra-long stable ovalbumin/sodium carboxymethylcellulose nanoparticle and loading properties of curcumin, Carbohydr. Polym. 271 (2021) 118451, https://doi.org/10.1016/j.carbpol.2021.118451.
[26] S. Solghi, Z. Emam-Djomeh, M. Fathi, F. Farahani, The encapsulation of curcumin by whey protein: assessment of the stability and bioactivity, J. Food Process Eng. 43 (2020) e13403, https://doi.org/10.1111/jfpe.13403.
[27] G. Xu, L. Li, X. Bao, P. Yao, Curcumin, casein and soy polysaccharide ternary complex nanoparticles for enhanced dispersibility, stability and oral bioavailability of curcumin, Food Biosci. 35 (2020) 100569, https://doi.org/10.1016/j.fbio.2020.100569.
[28] O. Madkhali, G. Mekhail, S.D. Wettig, Modified gelatin nanoparticles for gene delivery, Int. J. Pharm. 554 (2019) 224–234, https://doi.org/10.1016/j.ijpharm.2018.11.001.
[29] X. Feng, H. Dai, L. Ma, Y. Fu, Y. Yu, H. Zhou, T. Guo, H. Zhu, H. Wang, Y. Zhang, Properties of Pickering emulsion stabilized by food-grade gelatin nanoparticles: influence of the nanoparticles concentration, Colloids Surf. B: Biointerfaces 196 (2020) 111294, https://doi.org/10.1016/j.colsurfb.2020.111294.
[30] G. Kan, Y. Zi, L. Li, H. Gong, J. Peng, X. Wang, J. Zhong, Curcumin-encapsulated hydrophilic gelatin nanoparticle to stabilize fish oil-loaded Pickering emulsion, Food Chem. X. 17 (2023) 100590, https://doi.org/10.1016/j.fochx.2023.100590.
[31] G. Kan, Y. Zi, C. Shi, Y. Tan, H. Gong, X. Wang, J. Zhong, Interaction of curcumin with four types of gelatins in nanoparticles: mechanism and application for emulsion stabilization, Food Hydrocoll. 146 (2024) 109268, https://doi.org/10.1016/j.foodhyd.2023.109268.
[32] C. Tang, Nanocomplexation of proteins with curcumin: from interaction to nanoencapsulation (a review), Food Hydrocoll. 109 (2020) 106106, https://doi.org/10.1016/j.foodhyd.2020.106106.
[33] M.F. Sanner, Python: a programming language for software integration and development, J. Mol. Graph. Model. 17 (1999) 57–61.
[34] L.L.C. Schrödinger, The PyMOL Molecular Graphics System, Version 1.8, 2015.
[35] Y. Wang, L. Zhang, P. Wang, X. Xu, G. Zhou, pH-shifting encapsulation of curcumin in egg white protein isolate for improved dispersity, antioxidant capacity and

thermal stability, Food Res. Int. 137 (2020) 109366, https://doi.org/10.1016/j.foodres.2020.109366.
[36] R. Li, S. Wang, H. Feng, D. Zhuang, J. Zhu, An intelligent chitosan/gelatin film via improving the anthocyanin-induced color recognition accuracy for beef subfreshness differentiation monitoring, Food Hydrocoll. 146 (2024) 109219, https://doi.org/10.1016/j.foodhyd.2023.109219.
[37] Y. Zhang, A.N. Aryee, B.K. Simpson, Current role of in silico approaches for food enzymes, Curr. Opin. Food Sci. 31 (2020) 63–70, https://doi.org/10.1016/j.cofs.2019.11.003.
[38] C.-P. Racz, L.Z. Racz, C.G. Floare, G. Tomoaia, O. Horovitz, S. Riga, I. Kacso, G. Borodi, M. Sarkozi, A. Mocanu, C. Roman, M. Tomoaia-Cotisel, Curcumin and whey protein concentrate binding: thermodynamic and structural approach, Food Hydrocoll. 139 (2023) 108547, https://doi.org/10.1016/j.foodhyd.2023.108547.
[39] M. Stanca, C. Gaidau, T. Zaharescu, G.-A. Balan, I. Matei, A. Precupas, A. R. Leonties, G. Ionita, Physico-chemical changes induced by gamma irradiation on some structural protein extracts, Biomolecules 13 (2023) 774, https://doi.org/10.3390/biom13050774.
[40] H. Liu, B. Wang, C.J. Barrow, B. Adhikari, Relating the variation of secondary structure of gelatin at fish oil–water interface to adsorption kinetics, dynamic interfacial tension and emulsion stability, Food Chem. 143 (2014) 484–491, https://doi.org/10.1016/j.foodchem.2013.07.130.
[41] H. Yan, Y. Song, M. Yu, X. Yao, W. Zhang, Y. Xu, X. Li, Y. Xu, S. Fang, J. Qi, G. Xiong, C. Li, J. Jia, Y. Hu, Aspartic acid/arginine enhance the stability of gelatin emulsions, J. Food Eng. 361 (2024) 111735, https://doi.org/10.1016/j.jfoodeng.2023.111735.
[42] S. Li, X. Yang, Y. Zhang, H. Ma, Q. Liang, W. Qu, R. He, C. Zhou, G.K. Mahunu, Effects of ultrasound and ultrasound assisted alkaline pretreatments on the enzymolysis and structural characteristics of rice protein, Ultrason. Sonochem. 31 (2016) 20–28, https://doi.org/10.1016/j.ultsonch.2015.11.019.
[43] X. Zhou, X. Yu, F. Xie, Y. Fan, X. Xu, J. Qi, G. Xiong, X. Gao, F. Zhang, pH-responsive double-layer indicator films based on konjac glucomannan/camellia oil and carrageenan/anthocyanin/curcumin for monitoring meat freshness, Food Hydrocoll. 118 (2021) 106695, https://doi.org/10.1016/j.foodhyd.2021.106695.
[44] A. Etxabide, P.A. Kilmartin, J.I. Maté, Color stability and pH-indicator ability of curcumin, anthocyanin and betanin containing colorants under different storage conditions for intelligent packaging development, Food Control 121 (2021) 107645, https://doi.org/10.1016/j.foodcont.2020.107645.
[45] L. Dai, H. Zhou, Y. Wei, Y. Gao, D.J. McClements, Curcumin encapsulation in zein-rhamnolipid composite nanoparticles using a pH-driven method, Food Hydrocoll. 93 (2019) 342–350, https://doi.org/10.1016/j.foodhyd.2019.02.041.
[46] T. Yang, H. Yang, Y. Fan, B. Li, H. Hou, Interactions of quercetin, curcumin, epigallocatechin gallate and folic acid with gelatin, Int. J. Biol. Macromol. 118 (2018) 124–131, https://doi.org/10.1016/j.ijbiomac.2018.06.058.
[47] R. Mohammadi, M.A. Mohammadifar, M. Rouhi, M. Kariminejad, A. M. Mortazavian, E. Sadeghi, S. Hasanvand, Physico-mechanical and structural properties of eggshell membrane gelatin- chitosan blend edible films, Int. J. Biol. Macromol. 107 (2018) 406–412, https://doi.org/10.1016/j.ijbiomac.2017.09.003.
[48] N. Chaiwong, P. Leelapornpisid, K. Jantanasakulwong, P. Rachtanapun, P. Seesuriyachan, V. Sakdatorn, N. Leksawasdi, Y. Phimolsiripol, Antioxidant and moisturizing properties of carboxymethyl chitosan with different molecular weights, Polymers 12 (2020) 1445, https://doi.org/10.3390/polym12071445.
[49] H. Karimi-Maleh, S. Ranjbari, B. Tanhaei, A. Ayati, Y. Orooji, M. Alizadeh, F. Karimi, S. Salmanpour, J. Rouhi, M. Sillanpää, F. Sen, Novel 1-butyl-3-methyl-imidazolium bromide impregnated chitosan hydrogel beads nanostructure as an efficient nanobio-adsorbent for cationic dye removal: kinetic study, Environ. Res. 195 (2021) 110809, https://doi.org/10.1016/j.envres.2021.110809.
[50] X. Sun, Y. Sheng, K. Li, S. Sai, J. Feng, Y. Li, J. Zhang, J. Han, B. Tian, Mucoadhesive phenylboronic acid conjugated chitosan oligosaccharide-vitamin E copolymer for topical ocular delivery of voriconazole: synthesis, *in vitro/vivo* evaluation, and mechanism, Acta Biomater. 138 (2022) 193–207, https://doi.org/10.1016/j.actbio.2021.10.047.
[51] H. Haghighi, R. De Leo, E. Bedin, F. Pfeifer, H.W. Siesler, A. Pulvirenti, Comparative analysis of blend and bilayer films based on chitosan and gelatin enriched with LAE (lauroyl arginate ethyl) with antimicrobial activity for food packaging applications, Food Packag. Shelf Life 19 (2019) 31–39, https://doi.org/10.1016/j.fpsl.2018.11.015.
[52] Y. Liu, Y. Cai, X. Jiang, J. Wu, X. Le, Molecular interactions, characterization and antimicrobial activity of curcumin–chitosan blend films, Food Hydrocoll. 52 (2016) 564–572, https://doi.org/10.1016/j.foodhyd.2015.08.005.
[53] F. Babick, Chapter 3.2.1 - dynamic light scattering (DLS), in: V.-D. Hodoroaba, W. E.S. Unger, A.G. Shard (Eds.), Characterization of Nanoparticles, Elsevier, 2020, pp. 137–172, https://doi.org/10.1016/B978-0-12-814182-3.00010-9.
[54] W. Schärtl, Light Scattering From Polymer Solutions and Nanoparticle Dispersions, Springer Science & Business Media, 2007.
[55] Y. Dong, S. Zhao, W. Lu, N. Chen, D. Zhu, Y. Li, Preparation and characterization of enzymatically cross-linked gelatin/cellulose nanocrystal composite hydrogels, RSC Adv. 11 (2021) 10794–10803, https://doi.org/10.1039/D1RA00965F.
[56] F. Damiri, Y. Bachra, C. Bounacir, A. Laaraibi, M. Berrada, Synthesis and characterization of lyophilized chitosan-based hydrogels cross-linked with benzaldehyde for controlled drug release, J. Chem. 2020 (2020) e8747639, https://doi.org/10.1155/2020/8747639.
[57] F. Liu, H. Majeed, J. Antoniou, Y. Li, Y. Ma, W. Yokoyama, J. Ma, F. Zhong, Tailoring physical properties of transglutaminase-modified gelatin films by varying drying temperature, Food Hydrocoll. 58 (2016) 20–28, https://doi.org/10.1016/j.foodhyd.2016.01.026.
[58] L. Mao, L. Ma, Y. Fu, H. Chen, H. Dai, H. Zhu, H. Wang, Y. Yu, Y. Zhang, Transglutaminase modified type a gelatin gel: the influence of intra-molecular and inter-molecular cross-linking on structure-properties, Food Chem. 395 (2022) 133578, https://doi.org/10.1016/j.foodchem.2022.133578.
[59] D.J. Pochapski, C. Carvalho dos Santos, G.W. Leite, S.H. Pulcinelli, C.V. Santilli, Zeta potential and colloidal stability predictions for inorganic nanoparticle dispersions: effects of experimental conditions and electrokinetic models on the interpretation of results, Langmuir 37 (2021) 13379–13389, https://doi.org/10.1021/acs.langmuir.1c02056.